

mmCooper: A Multi-agent Multi-stage Communication-efficient and Collaboration-robust Cooperative Perception Framework

Bingyi Liu¹, Jian Teng¹, Hongfei Xue^{2*}, Enshu Wang^{3*}, Chuanhui Zhu¹, Pu Wang², Libing Wu³
¹Wuhan University Of Technology, ²University of North Carolina at Charlotte, ³Wuhan University

{byliu, tengjian, zhuchuanhui}@whut.edu.cn,

{hongfei.xue, Pu.Wang}@charlotte.edu, {wanges17, wu}@whu.edu.cn

Abstract

Collaborative perception significantly enhances individual vehicle perception performance through the exchange of sensory information among agents. However, real-world deployment faces challenges due to bandwidth constraints and inevitable calibration errors during information exchange. To address these issues, we propose mmCooper, a novel multi-agent, multi-stage, communication-efficient, and collaboration-robust cooperative perception framework. Our framework leverages a multi-stage collaboration strategy that dynamically and adaptively balances intermediate- and late-stage information to share among agents, enhancing perceptual performance while maintaining communication efficiency. To support robust collaboration despite potential misalignments and calibration errors, our framework captures multi-scale contextual information for robust fusion in the intermediate stage and calibrates the received detection results to improve accuracy in the late stage. We validate the effectiveness of mmCooper through extensive experiments on real-world and simulated datasets. The results demonstrate the superiority of our proposed framework and the effectiveness of each component.

1. Introduction

With the development of autonomous driving systems and Internet of Vehicles (IoVs) technologies, perception devices such as cameras and LiDARs have been widely deployed. Although perception, as a critical module in autonomous vehicles, has witnessed rapid advancements driven by deep learning-based algorithms, the traditional single-vehicle perception paradigms [19, 24, 45] cannot meet the safety and reliability requirements of autonomous vehicles due to unavoidable factors such as object occlusion and limitations in detection range [1, 4, 12, 22, 53].

Benefiting from infrastructure improvements and the advancement of communication technologies like V2X [20,

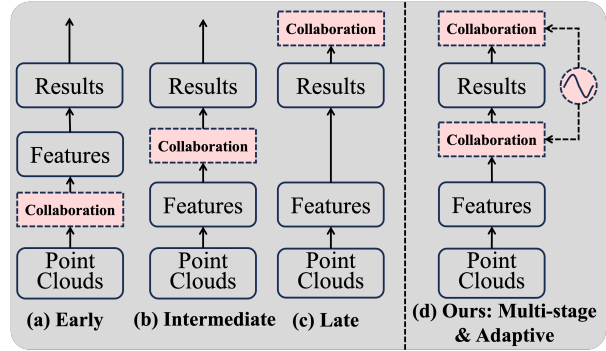


Figure 1. Comparison of different fusion approaches.

21], autonomous vehicles can achieve multi-vehicle collaborative perception by sharing perception information [3, 39], which significantly enhances the performance of perception systems. Although cooperative perception has made progress recently, its practical deployment still faces challenges such as communication resource constraints [6, 11], localization errors [25, 26] and low information fusion efficiency [38, 48].

In cooperative perception systems, the effectiveness of fusion strategies significantly affects both perception performance and communication efficiency. As illustrated in Figure 1 (a)-(c), the fusion strategies can be divided into three categories: early, intermediate, and late fusion methods, illustrated. Specifically, early fusion methods [5, 53] aggregate raw sensor observations from all agents, providing abundant information that can significantly enhance perception performance. However, transmitting raw sensor observations requires substantial bandwidth, making this approach costly for communication. Intermediate fusion methods [6, 11, 46–48] address this issue by sharing encoded features rather than raw data to reduce communication overhead. While effective, feature compression inevitably introduces information loss, which can compromise fusion accuracy. Late fusion methods [30, 32] on the other hand, minimize communication demands by sharing lightweight perception results among agents. However,

*Corresponding authors

this approach is highly sensitive to environmental noise, as even minor disturbances can degrade collaborative quality. Overall, these above single-stage cooperative perception approaches face challenges in managing the trade-off between perception accuracy and communication efficiency, raising a compelling question: *can we improve the perception performance while preserving communication efficiency by strategically sharing information across multiple stages to harness the strengths of each fusion stage?*

In addition, the data exchanged by agents inevitably experiences misalignment and contains calibration errors during the synchronization process due to communication delays and pose noise [13, 33]. These calibration errors can produce misleading features and proposals in subsequent steps, thereby affecting the performance of the perception system. While existing intermediate fusion methods attempt to address the calibration errors through position-wise feature fusion [16, 18, 23], they often overlook the critical role of neighboring region information for enhancing collaborative robustness. Meanwhile, late fusion methods [2, 28, 34] simply merge bounding boxes from collaborative agents, failing to leverage information-rich intermediate features from the ego agent, which could help refine and calibrate these bounding boxes for higher accuracy.

To this end, we propose **mmCooper**, a novel multi-agent, multi-stage, communication-efficient, and collaboration-robust **cooperative** perception framework. The proposed mmCooper framework facilitates effective information aggregation across fusion stages and enhances communication efficiency through carefully designed core components. Specifically, we design an adaptive multi-stage data fusion mechanism that facilitates multi-agent cooperation by dynamically fusing information at both intermediate and late stages, as shown in Figure 1. Guided by a confidence-based filtering gaile strategy, this mechanism automatically assesses and determines the data volume to be processed at intermediate and late stages. High-confidence bounding boxes are shared directly, while intermediate features are selectively shared instead of bounding boxes for regions requiring further contextual reference, and low-confidence areas are excluded to prevent propagating misleading information. This dual-stage fusion approach enhances perception performance while maintaining communication efficiency.

Besides, to further address potential misalignment and calibration noise among agents, we incorporate specific designs in the proposed mmCooper framework for both intermediate and late stages. In the intermediate stage, we introduce a Multi-scale Offset-aware Fusion Module that not only fuses data from target locations related to cooperative agents’ views but also from nearby regions, adding redundancy to mitigate calibration noise. For the late stage, we design a Bounding Box Filtering & Calibration

Module that uses the information-rich intermediate-stage features from the ego agent to filter inaccurate bounding boxes received from other agents and refine the remaining noisy ones. By integrating these corrected and ego-generated bounding boxes, our mmCooper framework is able to achieve high perception accuracy and robustness. We evaluated the performance of our mmCooper framework on both real and virtual datasets, including DAIR-V2X [49], OPV2V [43] and V2XSet[42]. Experimental results demonstrate that mmCooper outperforms previous methods across various settings, confirming its effectiveness as a communication-efficient and robust multi-stage cooperative perception framework. To summarize, our main contributions are summarized as follows:

- We propose mmCooper, a multi-agent multi-stage communication-efficient collaboration-robust cooperative perception framework. To our knowledge, this is the first framework to address the tradeoff between limited communication bandwidth and desired perception performance by sharing both intermediate and late-stage information for multi-agent collaborative perception.
- To address the potential misalignment and calibration error among agents, we incorporate a Multi-scale Offset-aware Fusion Module to integrate spatially adjacent contextual information at different feature scales in the intermediate stage and a Bounding Box Filtering & Calibration Module to filter and improve the bounding boxes from other agents in the late stage, guided by the information-rich intermediate features.
- Extensive experiments show excellent performance on both real-world and simulated datasets, with a 7.29%/1.31%/2.09% improvement in AP@0.7 on OPV2V, DAIR-V2X and V2XSet datasets over the second-best state-of-the-art methods. Additionally, our approach requires only 1/9153, 1/156 and 1/18305 of the communication volume used by comparable methods.

2. Related Work

2.1. Multi-Agent Communication

Communication strategies in multi-agent systems have been widely studied [31]. Early works [17, 29, 36] often used predefined protocols or heuristic methods to determine how agents communicate with each other. However, these methods are difficult to generalize to complex tasks. Recently, several learning-based communication strategies have been proposed to adapt to diverse scenario applications. For instance, Vain [10] utilizes attention neural structures to specify the information that needs to be shared in agent interactions. ATOC [14] introduces recurrent units to decide who agents communicate with by receiving local observations and action intentions from other agents. TarMAC [7] designs an architecture oriented towards reinforcement learning, learning to communicate from task-specific rewards.

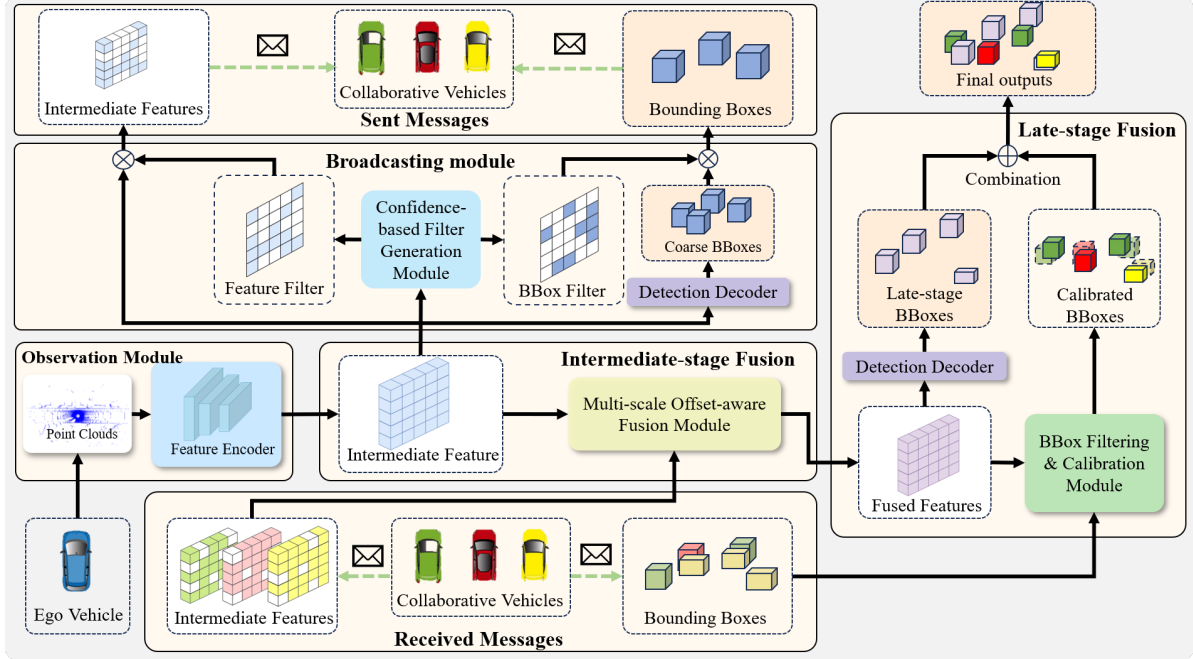


Figure 2. Overview of mmCooper framework: a cooperative perception system with adaptive multi-stage fusion.

CommNet [35] learns continuous communication in multi-agent systems. Most of these previous works have considered decision-making tasks and have employed reinforcement learning due to the lack of explicit supervision. Different from these works, our paper focuses on LiDAR-based 3D perception tasks in complex autonomous driving scenarios and achieves efficient communication between agents using a multi-stage communication strategy.

2.2. Collaborative Perception

Collaborative perception addresses the limitations of single-agent perception by aggregating perception information from surrounding agents to adapt to complex and dynamic autonomous driving environments. Current work is categorized into early, intermediate, and late fusion based on collaboration stages. Early fusion [5, 51, 53] shares raw point cloud data among agents, achieving high perception performance but consuming significant bandwidth resources. EMP [53] achieved scalability and adaptability on highly fluctuating open roads by dynamically partitioning the point cloud range shared by agents. Late fusion [30, 32, 44] shares lightweight proposals between agents but performs poorly and is sensitive to noise. VIPS [30] implemented efficient graph-structured matching to enable object-level fusion. Intermediate fusion [11, 18, 23, 42, 50] shared features among agents, yet complete Intermediate features still incur high bandwidth consumption. Recent work focused on novel communication mechanisms to filter Intermediate features and reduce communication volume. For instance, Where2comm [11] employed a confidence-based scheme to guide agents in focusing on sharing spatially critical in-

formation. ERMVP [50] adopted a hierarchical feature sampling strategy to reduce communication overhead while leveraging sparse consensus features to mitigate localization errors. Different from these works, our framework conducts multi-stage fusion instead of single-stage which balances the perception performance and communication overhead. As far as we know, only a few works have considered multi-stage settings. Zhang *et al.* [52] proposes a defense method that combines raw data and intermediate features to fuse redundant information, thereby reducing the impact of spurious data. Zhao *et al.* [54] simultaneously considers early raw data and late-stage detection results to address malicious agents in collaborative environments. However, both works focus on security issues related to collaborative perception instead of improving sensing performance. Xie *et al.* [40] applies reinforcement learning for dynamic partitioning of early, intermediate, and late-stage information. However, this work merely divides the data without integrating information across stages. In contrast to these works, this paper introduces a collaborative perception framework that aims to improve sensing performance by conducting multi-stage data fusion.

3. Methodology

3.1. Overview

This section introduces our proposed mmCoop framework, as illustrated in Figure 2, which comprises four main components: the Observation Module, the Broadcasting Module, the Intermediate-stage Fusion, and the Late-stage Fusion. The Observation Module (Sec.3.2) serves as the foundation by extracting essential features from the ego ve-

hicle’s LiDAR-based point cloud data. The Broadcasting Module (Sec.3.3) includes a Detection Decoder to generate coarse bounding boxes from intermediate features, along with a Confidence-based Filter Generation Module to produce filters that dynamically determine the data volume shared at the intermediate and late stages. These generated filters enable adaptive data sharing: high-confidence bounding boxes are shared directly, intermediate features are selectively transmitted for areas needing additional context, and low-confidence areas are excluded, balancing perception accuracy with communication efficiency. The Intermediate-stage Fusion (Sec.3.4) contains the Multi-scale Offset-aware Fusion Module, which uses cross-attention to integrate features from both target and nearby regions for robust feature fusion. In the Late-stage Fusion (Sec.3.5), a Bounding Box Filtering and Calibration Module filters inaccurate bounding boxes from other agents and calibrates the remaining ones using the ego agent’s intermediate features. The Late-stage Fusion contains the Bounding Box Filtering and Calibration Module to filter out inaccurate bounding boxes received from other agents and refine the remaining noisy ones by leveraging the information-rich intermediate features from the ego agent. Then, the calibrated bounding boxes from all other agents will be combined with the bounding boxes generated by the ego agent to produce the final prediction.

3.2. Observation Module

In a multi-agent cooperative perception scenario, consider the collaboration of n agents, represented by the agent set $N = \{1, \dots, n\}$. One vehicle serves as the ego vehicle and the remaining $n - 1$ agents act as collaborators. The ego vehicle aggregates information from the collaborators to achieve cooperative perception. Considering the i -th agent as the ego vehicle, for the j -th collaborator, where $i, j \in N$, the point cloud observation is given as X_j . The ego vehicle first broadcasts its basic information to the collaborators, such as coordinates and heading angle. The collaborators utilize this basic information to project their point cloud observations into the ego vehicle’s coordinate system, with the projected point cloud observation represented as $x'_j = T_{j \rightarrow i} \cdot x_j$, where $T_{j \rightarrow i}$ denotes the transformation matrix from agent j to agent i . Subsequently, each agent extracts features from its point cloud observation through a shared encoder to obtain Bird’s Eye View (BEV) features, represented as $F_{bev}^k = \psi_{encoder}(x_k) \in \mathbb{R}^{C \times H \times W}$, where $\psi_{encoder}$ denotes the shared PointPillar encoder [15], and $k \in N$, and C , H , and W correspond to the channel, height, and width of the feature map, respectively.

3.3. Broadcasting Module

For the locally encoded BEV features, prior work has mainly focused on either directly sharing intermediate-stage features or decoding them to obtain late-stage bounding

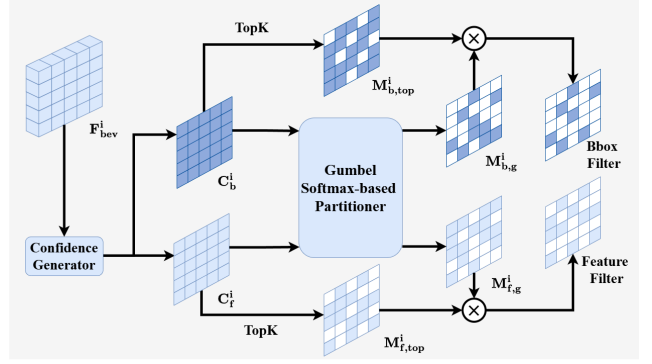


Figure 3. The Confidence-based Filtering Generation Module

boxes, which are then shared. However, collaboration schemes based on a single stage often struggle to effectively balance communication bandwidth and perception performance. To effectively leverage the advantages of multi-stage data, we introduce a multi-stage collaboration framework that simultaneously balances bandwidth and accuracy by transferring filtered features and proposals between agents. As shown in Figure 3, our Broadcasting Module filters the intermediate features and initially generates coarse bounding boxes, which are then transmitted to other agents.

Confidence-based Filter Generation Module. The Confidence-based Filter Generation Module, as a key component of the Broadcasting Module, serves two main purposes: 1) dynamically and adaptively determining the allocation of features and coarse bounding boxes; 2) ensuring that the discrete operations involved in obtaining the filter can still propagate gradients properly. To filter spatial features and bounding boxes, we input the encoded features into the Confidence Generator to generate spatial confidence maps for both the features and proposals. The confidence maps represent the potential regions of objects and are denoted as:

$$C_f^i, C_b^i = \phi_{conf}(F_{bev}^i),$$

where $\phi_{conf}(\cdot)$ refers to the Multi-stage Confidence Generator, and C_f^i, C_b^i represents the confidence maps for the features and proposals, respectively. A Gaussian Filter is then applied to the spatial confidence maps, helping to filter out anomalous areas and incorporate contextual effects, thereby enhancing the robustness of critical region selection. To eliminate irrelevant background information, the top $m\%$ highest-confidence positions are selected from each confidence map to generate the spatial filter $M_{f/b,top}^i$. Then we add Gumbel noise $g_{f/b}$ to the confidence maps to introduce a certain level of randomness, expressed as:

$$g_{f/b} = -\log(-\log u), u \sim Uniform(0, 1).$$

The introduction of Gumbel noise can enhance the exploratory nature of the model and improve its generalization capability. For the same positions in the confidence maps from two stages, we retain only the parts with relatively

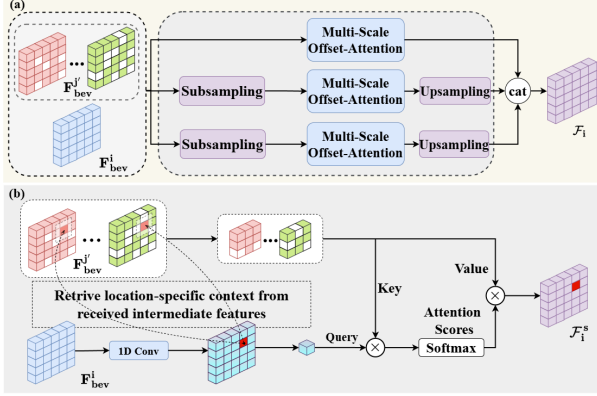


Figure 4. (a) The Multi-scale Offset-aware Fusion Module. (b) The Multi-scale Offset-aware Attention Module.

high confidence scores. The confidence score indicates the potential location of an object. When a high-dimensional bounding box exhibits high confidence in representing the object, the agent will share the bounding box. Otherwise, intermediate-stage features are required to convey the information at that location. In addition, to ensure the continuity of the dynamic allocation process for the intermediate-stage features and coarse bounding boxes, we employ the Gumbel Softmax method to obtain approximate samples from a discrete distribution. Utilizing the straight-through estimator to acquire discrete distributions while preserving standard forward propagation. The specific process is represented as follows:

$$M_{f/b,g}^i = f_{max} \left(\frac{\exp((\log C_{f/b} + g_f)/\tau)}{\sum_s \exp((\log C_s + g_s)/\tau)} \right),$$

where τ denotes the temperature parameter of the distribution ($\tau > 0$), and $s \in \{f, b\}$. Based on the above process, our final filter $M_{f/b}^i$ is represented as:

$$M_{f/b}^i = M_{f/b,g}^i \odot M_{f/b,top}^i,$$

3.4. Intermediate-stage Fusion

The data shared between agents inevitably contains calibration errors, which cause misalignment of feature maps. These errors may lead to the ego vehicle misjudging the positions of surrounding objects, thereby reducing detection performance. To address these issues, we implement a novel Multi-scale Offset-aware Fusion (MOF) Module in the intermediate-stage Module. By aggregating information from surrounding positions, the per-position feature fusion process introduces redundancy, allowing it to effectively tolerate calibration errors.

Multi-scale Offset-aware Fusion. The overall pipeline of this module is shown in Figure 4(a). First, the ego features and the received collaborator features are encoded into three scales to capture target information of varying sizes.

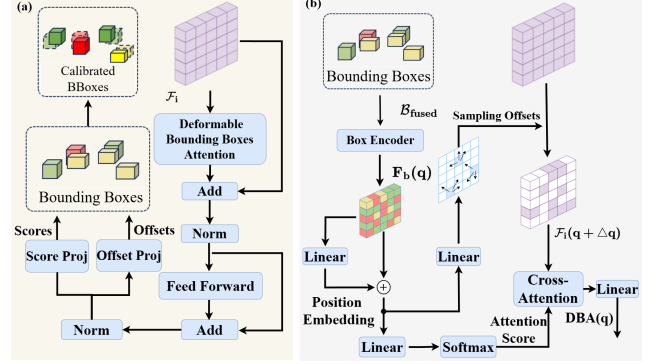


Figure 5. (a) The BBox Filtering & Calibration Module. (b) The Deformable Bounding Box Attention Module.

Then, our multi-scale offset-aware attention is applied for feature fusion. Upsampling is performed on different scales to obtain fused features of the same size. The details of the Multi-scale Offset-aware Attention Module are shown in Figure 4(b). We encode the ego features into queries via a convolutional layer, and employ the spatially continuous features at the query positions of each collaborator’s features as keys and values in the cross-attention mechanism. Define the specified location as (i, j) on the feature map, with a neighborhood size of $s \times s$. The output representation of feature fusion at location c is expressed as:

$$F_{i,c} = CrossAttn(\sigma(F_{bev,c}^i), F_{bev,c}^{j,s \times s}, F_{bev,c}^{j,s \times s}),$$

Where σ denotes a 1D convolutional layer, $F_{bev,c}^{j,s \times s}$ represents the collaborator features within an $s \times s$ neighborhood centered at position (i, j) , and m denotes the ego feature at position (i, j) . For the feature at position (i, j) on the ego feature map, we consider the collaborator feature at this location and the features within its neighborhood as keys and values. By selectively aggregating the features at this position and its neighborhood, we achieve collaboratively-robust feature fusion.

3.5. Late-stage Fusion

Due to the limited perception capabilities of individual agents, they often generate imprecise or even incorrect bounding boxes. Existing late-stage fusion methods focus only on the fusion strategy at the current stage. By utilizing data sharing across multiple stages, we are able to fully utilize the abundant intermediate fused features to calibrate the received bounding boxes.

BBox Filtering & Calibration Module. In this module, we propose a Feature-guided Bounding Boxes Calibration Transformer (FBCFormer) to calibrate the bounding boxes transmitted by collaborators and filter out erroneous ones. As depicted in Figure 5(a), we use the received bounding boxes from collaborators and the intermediate-stage fused features as inputs to the Deformable Bounding Boxes At-

tention (DBA) Module. The remaining components follow the vanilla transformer setup [37]. We apply score and offset projections to the output of the FBCFormer to learn the scores and offsets for each bounding box, thereby removing incorrect bounding boxes and calibrating the coarse ones.

Figure 5(b) provides a detailed illustration of our DBA module. We first encode the bounding boxes received from collaborators. By applying our bounding boxes encoder to the bounding box coordinates, size, and orientation information, we effectively extract the bounding box feature. We use a deformable cross-attention module to focus on keypoints information, which yields a robust representation of bounding box errors. Specifically, the bounding box features serve as the initial query embedding q , and the bounding box coordinates act as reference points. A linear layer encodes each bounding box’s coordinates into position embeddings. Subsequently, the linear layer learns the 2D spatial offsets for each reference point, extracting keypoints information at $q + \Delta q$. The cross-attention layer aggregates keypoint information from multiple collaborator features to enhance the representation for each query embedding:

$$DBA(q) = \sum_{\alpha=1}^A W_{\alpha} \left[\sum_{n=1}^N \sum_{m=1}^M \omega(W_{\beta} F_b(q)) F_j(q + \Delta q_m) \right],$$

where A is the number of attention heads, $W_{\alpha/\beta}$ are learnable parameters, m represents the number of keypoints, and ω denotes the softmax operation. Finally, two linear layers are learned to determine the offsets and scores for each bounding box. The offsets are used to adjust the position, size, and angle of each bounding box, while the scores are filtered using a threshold selection function $f_{sel}(\cdot)$ to discard lower-scoring bounding boxes. To prevent learning unreasonable offsets and scores, we control the output range using the tanh activation function. Additionally, to train our FBCFormer component, we compute the offset loss \mathcal{L}_{off} using the smooth absolute error loss between the detected bounding boxes and the corresponding ground truth bounding boxes with the same identifier. The score loss \mathcal{L}_{score} is calculated using focal loss.

3.6. Loss Functions

We use two detection decoders to perform regression and classification on the fused features. The regression output represents the position, size, and yaw angle of each predefined box, expressed as $O_{reg} = f_{dec}^r(\mathcal{F}_i) \in \mathbb{R}^{7 \times H \times W}$. The classification output indicates the confidence score for each predefined box, represented as $O_{cls} = f_{dec}^c(\mathcal{F}_i) \in \mathbb{R}^{2 \times H \times W}$. To optimize the proposed system, we use smooth absolute error loss for regression and focal loss for classification, denoted as \mathcal{L}_{reg} and \mathcal{L}_{cls} , respectively. Combining the above losses, our total loss is represented as:

$$\mathcal{L} = \mathcal{L}_{reg} + \mathcal{L}_{cls} + \mathcal{L}_{off} + \mathcal{L}_{score}.$$

4. Experiments

4.1. Datasets and experimental settings

Datasets. We conduct extensive validation of our proposed mmCooper on three benchmark datasets, namely OPV2V [43], DAIR-V2X [49] and V2XSet[42]. OPV2V is the first large-scale public V2V cooperative perception simulation dataset, collected using the autonomous driving simulator CARLA [8] and the cooperative driving simulation framework OpenCDA [41]. This dataset includes 6 types of road scenarios and 9 different cities. It comprises 73 different scenes, 11,464 frames of point clouds and RGB images, and over 230,000 annotated 3D detection boxes. The training, validation, and test sets are divided into 6,374, 1,980, and 2,170 frames, respectively. DAIR-V2X is a comprehensive large-scale real-world 3D object detection dataset designed for vehicle-road cooperative autonomous driving research. This dataset includes 71,254 frames of point cloud and image data, with the training, validation, and test sets split in a 5:2:3 ratio. The V2XSet dataset is a large-scale synthetic dataset designed for V2X perception. It consists of 73 scenarios collected using CARLA and OpenCDA. It contains a total of 11,447 frames, with each frame involving up to five agents. The dataset is divided into training, validation, and test sets, consisting of 6,694, 1,920, and 2,833 frames, respectively.

Evaluation metrics. To evaluate the 3D object detection performance of the baseline and the proposed framework, we use the average precision (AP) [9] at Intersection-over-Union (IoU) thresholds of 0.5 and 0.7 as the evaluation metric. The communication volume between agents is expressed by the following equation:

$$\mathbf{V}_{comm} = \log_2 ((|M| \times H \times W \times C + N_{bbx} \times 7) \times 32/8),$$

where $|M|$ represents the feature retention ratio, N_{bbx} denotes the number of bounding boxes per agent, and 7 is used to describe the coordinates, dimensions, and angle information of each bounding box. Each value is represented using the float32 data type, with division by 8 converting the result to bytes.

Implementation details. We implement our model on the PyTorch toolbox [27] and train it on NVIDIA GeForce RTX 4090 GPUs. We use the Adam optimizer and adopt batch sizes of 3, 5, and 3 for the OPV2V, DAIR-V2X, and V2XSet datasets, respectively, with 60 epochs for each. All models use the PointPillars [15] backbone to extract features from the raw point clouds. The confidence ratio selected for the Confidence-based Filter Generation Module is 70% for OPV2V, 60% for DAIR-V2X, and 70% for V2XSet, and the surrounding grid size chosen for the Multi-scale Offset-aware Attention is 3x3. To closely simulate real traffic conditions, we introduce localization and heading errors with standard deviations of 0.2 m and 0.2°, respectively, sampled from a Gaussian distribution into the initial state of each

Models	Venue	OPV2V		DAIR-V2X		V2XSet	
		Comm (log2)(↓)	AP@ 0.7/0.5 (↑)	Comm (log2)(↓)	AP@ 0.7/0.5 (↑)	Comm (log2)(↓)	AP@ 0.7/0.5 (↑)
No Fusion* [15]	CVPR 2019	-	48.66/68.71	-	43.57/50.03	-	40.20/60.60
Late Fusion* [15]	CVPR 2019	10.36	59.48/79.62	9.08	34.47/51.14	10.26	30.75/54.92
Intermediate Fusion* [15]	CVPR 2019	23.22	<u>70.82/ 88.41</u>	22.62	39.38/56.22	23.22	59.38/83.18
When2com [23]	CVPR 2020	23.22	57.55/74.11	22.62	33.68/48.20	23.22	41.85/67.41
DisoNet [18]	NIPS 2021	23.22	68.64/84.72	22.62	40.69/52.67	23.22	54.11/79.82
Where2comm [11]	NIPS 2022	23.22	69.73/85.16	22.62	43.71/59.52	23.22	<u>63.77/83.17</u>
V2X-ViT [42]	ECCV 2022	23.22	70.06/84.65	22.62	40.43/53.08	23.22	61.49/83.63
ERMVP [50]	CVPR 2024	22.46	64.60/85.81	21.98	<u>46.96/64.21</u>	18.46	58.47/81.14
Ours	-	10.09	78.11/ 88.93	<u>15.33</u>	48.27/ 65.12	9.06	65.86/84.40

Table 1. Collaborative perception performance on the OPV2V, DAIR-V2X and V2XSet dataset with a time delay of 100 *ms*, localization errors of 0.2 *m*, and heading errors of 0.2° using Average Precision(AP)@0.7/0.5 as metrics. *Comm* denotes the communication volume. **Bold numbers** indicate the best results, while underlined numbers represent the second-best results. * represents a variation of PointPillar [15].

agent. The communication range is set to 70 *m*. Agents beyond the communication range do not participate in the collaborative process.

4.2. Quantitative Evaluation

Detection Performance Evaluation. Table 1 presents the comparison of the perception performance of our proposed mmCooper model and various baseline models on the OPV2V, DAIR-V2X and V2XSet datasets with a time delay of 100 *ms*, localization errors of 0.2 *m*, and heading errors of 0.2°. The baseline models included in the comparison are described as follows. The No Fusion model relies solely on local observations for 3D object detection. Late Fusion shares the perception results of individual predictions among agents. Intermediate Fusion allows agents to share complete features extracted from raw point clouds. The above three models are all variants based on the PointPillar[15] point cloud detector. Additionally, we consider state-of-the-art (SOTA) models, including When2com [23], DisoNet [18], Where2comm [11], V2XViT [42] and ERMVP [50]. As shown in the table, our proposed mmCooper outperforms previous methods on both simulated and real-world datasets, demonstrating the effectiveness of our approach. Compared to existing SOTA models, mmCooper outperforms the second-best baseline on the OPV2V, DAIR-V2X, and V2XSet datasets by 7.29%/0.59%, 1.31%/0.91% and 2.09%/0.77% in AP@0.7/0.5, respectively. Notably, mmCooper significantly reduces communication costs, achieving levels comparable to late fusion on both datasets. In comparison to other models, the communication volume required to achieve optimal performance is 9153/156/18305 times that of our method. On the OPV2V dataset, our method even achieves lower communication volume than late fusion. A possible explanation is that our Confidence-based Filter Generation Module first removes low-quality features and bounding boxes, then dynamically allocates intermediate-stage features and late-stage bounding boxes based on this. The dynamic allocation process prioritizes using bounding

boxes to convey information, preserving a few key features while eliminating a large amount of background information.

Robustness to Localization Errors and Transmission Delay. We verified the robustness of the agents during collaborative processes in the presence of localization errors and transmission delay on the OPV2V and DAIR-V2X datasets. Following the noise settings in [42], localization noise was sampled from a Gaussian distribution with a mean of 0 *m* and a standard deviation $\sigma \in \{0, 0.2, 0.4\}m$. As shown in table 2, as the standard deviation of the localization noise gradually increases, the detection performance of the models correspondingly decreases. On the DAIR-V2X dataset, when2com even performs worse than the No Fusion method when the localization error exceeds 0.2 *m*. Our method outperforms previous SOTA models under all localization noise settings, effectively demonstrating its robustness to varying levels of localization error. Transmission delay can lead to misalignment of features and proposals, thereby impacting detection performance. We evaluated the models on the OPV2V and DAIR-V2X datasets with time delays $\tau \in \{0, 200, 400\}ms$ set to 0 *ms*, 200 *ms*, and 400 *ms*. With increasing time delay, the detection performance of all methods gradually degrades due to misleading features and proposals. However, mmCooper achieves higher Average Precision (AP) than current SOTA models on both datasets. This robustness to localization errors and transmission delay demonstrates that considering spatial continuity aligns features effectively, and intermediate-stage features provide significant guidance for subsequent bounding boxes.

4.3. Ablation Study

We conducted comprehensive ablation studies on the OPV2V and DAIR-V2X datasets to demonstrate the importance of different designs, with the ablation results shown in Table 3.

Importance of Core Components. All our core components contribute to performance improvement. Remov-

Noise Type	Localization Errors(m)						Transmission Delay(ms)					
Datasets	OPV2V			DAIR-V2X			OPV2V			DAIR-V2X		
Noise Level	0.0	0.2	0.4	0.0	0.2	0.4	0	200	400	0	200	400
No Fusion	48.66	48.66	48.66	43.57	43.57	43.57	48.66	48.66	48.66	43.57	43.57	43.57
When2com [23]	70.82	64.35	59.98	39.50	36.62	35.03	70.82	43.96	36.55	39.50	36.83	33.72
DiscoNet [18]	76.05	73.59	65.85	46.94	46.03	44.96	76.05	60.08	50.33	46.94	44.03	41.57
Where2comm [11]	78.47	75.45	69.77	52.34	49.34	46.96	78.47	65.23	53.33	52.34	47.76	45.25
V2XViT [42]	77.83	75.21	66.72	46.12	43.81	42.53	77.83	66.08	50.33	46.12	45.49	43.99
ERMVP [50]	<u>80.55</u>	<u>76.19</u>	<u>72.78</u>	<u>53.27</u>	48.66	45.97	<u>80.55</u>	<u>68.89</u>	<u>68.31</u>	<u>53.27</u>	<u>49.68</u>	<u>48.60</u>
Ours	86.41	82.53	76.80	56.06	51.52	47.66	86.41	77.44	75.26	56.06	50.96	50.81

Table 2. Results for different localization errors (m) and transmission delay (ms) on the OPV2V and DAIR-V2X dataset evaluated using AP@0.7. **Bold numbers** indicate the best results, while underlined numbers represent the second-best results.

GSP	MOA	FBCFormer	LF	IF	AP@0.7/0.5(↑)	
					OPV2V	DAIR-V2X
✓	✓	✓	✓	✓	78.11/88.93	48.27/65.12
Importance Of Core Components						
✗	✓	✓	-	-	73.46/88.84	47.66/63.63
✓	✗	✓	-	-	72.60/88.51	47.27/63.49
✓	✓	✗	-	-	76.77/88.56	44.31/59.68
Results of Single-stage Fusion						
-	-	-	✗	✓	76.83/88.65	44.11/59.92
-	-	-	✓	✗	66.80/78.62	46.21/57.02

Table 3. Ablation study results of different designs in mmCooper on the OPV2V and DAIR-V2X datasets. GSP: Gumbel Softmax-based Partitioner; MOA: Multi-scale Offset-aware Attention; FBCFormer: Feature-guided Bounding Boxes Calibration Transformer; LF: Late-stage Fusion; IF: Intermediate-stage Fusion.

ing the Gumbel Softmax-based Partition (GSP) from the Confidence-based Filter Generation Module leads to a performance drop. This indicates that low-quality information exists in the intermediate-stage features and the late-stage bounding boxes, potentially due to irrelevant background or noise. Introducing adaptive and dynamic allocation for intermediate-stage features and late-stage bounding boxes effectively filters out irrelevant information. The absence of the intermediate-stage multi-scale Offset-aware Attention (MOA) module and the late-stage Feature-guided Bounding Boxes Calibration Transformer (FBCFormer) module also leads to a loss of accuracy, demonstrating that incorporating spatial neighborhood information and cross-stage calibration modules effectively addresses potential misalignment and calibration noise.

Results of Single-stage Fusion. We entirely removed the Late Fusion (LF) and the Intermediate Fusion (IF) separately to degrade our model to single-stage fusion. The experimental results indicate that removing either module leads to a performance decline, underscoring the effectiveness of the proposed multi-stage cooperation approach.

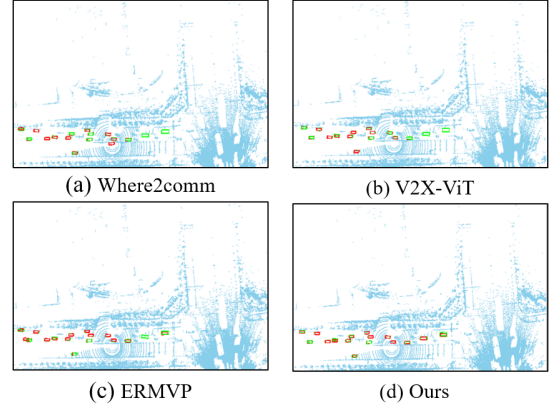


Figure 6. Visualization comparison of detection results on the DAIR-V2X dataset. Green and red boxes represent the ground truth and the model-predicted bounding boxes, respectively.

4.4. Qualitative Evaluation

Visualization of Detection Results. To visually display the detection results of our proposed mmCooper and the other baseline models, Figure 6 shows the visualization results for two scenarios in the DAIR-V2X dataset. Compared to SOTAs, our mmCooper achieves high-precision 3D object detection in these challenging scenarios, almost correctly predicting all ground truth. Specifically, the advantages of our method stem from two aspects: 1) The proposed dynamic adaptive allocation strategy enables dynamic partitioning of intermediate-stage features and late-stage bounding boxes, effectively filtering out irrelevant and noisy information. 2) Our Multi-scale Offset-aware Attention Module and BBox Filtering & Calibration Module effectively address misalignment and calibration noise.

5. Conclusion

In this paper, we have proposed mmCooper, a novel multi-agent, multi-stage, communication-efficient, and collaboration-robust cooperative perception framework. mmCooper is the first framework to achieve adaptive fusion of complementary data across stages for cooperative perception. We introduce the Confidence-based Filter Generation Module to enable dynamic partitioning of intermediate features and late-stage bounding boxes, bal-

ancing communication load and perception performance. Additionally, the Multi-scale Offset-aware Fusion module and BBox Filtering & Calibration module are incorporated to address potential misalignment and calibration noise among agents. mmCooper outperforms the second-best state-of-the-art models on the OPV2V, DAIR-V2X, and V2Xset datasets, achieving improvements of 7.29%, 1.31%, and 2.09% in AP@0.7, respectively, while reducing communication volume by factors of 9153, 156 and 18305.

References

- [1] Christoph Allig and Gerd Wanielik. Alignment of perception information for cooperative perception. In *2019 IEEE Intelligent Vehicles Symposium (IV)*, pages 1849–1854. IEEE, 2019. 1
- [2] Kunyang Cai, Ting Qu, Bingzhao Gao, and Hong Chen. Consensus-based distributed cooperative perception for connected and automated vehicles. *IEEE Transactions on Intelligent Transportation Systems*, 24(8):8188–8208, 2023. 2
- [3] Cheng Chang, Jiawei Zhang, Kunpeng Zhang, Wenqin Zhong, Xinyu Peng, Shen Li, and Li Li. Bev-v2x: Cooperative birds-eye-view fusion and grid occupancy prediction via v2x-based data sharing. *IEEE Transactions on Intelligent Vehicles*, 2023. 1
- [4] Guoying Chen, Xuanming Zhao, Zhenhai Gao, and Min Hua. Dynamic drifting control for general path tracking of autonomous vehicles. *IEEE Transactions on Intelligent Vehicles*, 8(3):2527–2537, 2023. 1
- [5] Qi Chen, Sihai Tang, Qing Yang, and Song Fu. Cooper: Cooperative perception for connected autonomous vehicles based on 3d point clouds. In *2019 IEEE 39th International Conference on Distributed Computing Systems (ICDCS)*, pages 514–524. IEEE, 2019. 1, 3
- [6] Ziming Chen, Yifeng Shi, and Jinrang Jia. Transiff: An instance-level feature fusion framework for vehicle-infrastructure cooperative 3d detection with transformers. In *Proceedings of the IEEE/CVF International Conference on Computer Vision*, pages 18205–18214, 2023. 1
- [7] Abhishek Das, Théophile Gervet, Joshua Romoff, Dhruv Batra, Devi Parikh, Mike Rabbat, and Joelle Pineau. Tarmac: Targeted multi-agent communication. In *International Conference on machine learning*, pages 1538–1546. PMLR, 2019. 2
- [8] Alexey Dosovitskiy, German Ros, Felipe Codevilla, Antonio Lopez, and Vladlen Koltun. Carla: An open urban driving simulator. In *Conference on robot learning*, pages 1–16. PMLR, 2017. 6
- [9] Mark Everingham, Luc Van Gool, Christopher KI Williams, John Winn, and Andrew Zisserman. The pascal visual object classes (voc) challenge. *International journal of computer vision*, 88:303–338, 2010. 6
- [10] Yedid Hoshen. Vain: Attentional multi-agent predictive modeling. *Advances in neural information processing systems*, 30, 2017. 2
- [11] Yue Hu, Shaoheng Fang, Zixing Lei, Yiqi Zhong, and Siheng Chen. Where2comm: Communication-efficient collaborative perception via spatial confidence maps. *Advances in neural information processing systems*, 35:4874–4886, 2022. 1, 3, 7, 8
- [12] Min Hua, Guoying Chen, Buyang Zhang, and Yanjun Huang. A hierarchical energy efficiency optimization control strategy for distributed drive electric vehicles. *Proceedings of the Institution of Mechanical Engineers, Part D: Journal of Automobile Engineering*, 233(3):605–621, 2019. 1
- [13] Tao Huang, Jianan Liu, Xi Zhou, Dinh C Nguyen, Mostafa Rahimi Azghadi, Yuxuan Xia, Qing-Long Han, and Sumei Sun. V2x cooperative perception for autonomous driving: Recent advances and challenges. *arXiv preprint arXiv:2310.03525*, 2023. 2
- [14] Jiechuan Jiang and Zongqing Lu. Learning attentional communication for multi-agent cooperation. *Advances in neural information processing systems*, 31, 2018. 2
- [15] Alex H Lang, Sourabh Vora, Holger Caesar, Lubing Zhou, Jiong Yang, and Oscar Beijbom. Pointpillars: Fast encoders for object detection from point clouds. In *Proceedings of the IEEE/CVF conference on computer vision and pattern recognition*, pages 12697–12705, 2019. 4, 6, 7
- [16] Jinlong Li, Runsheng Xu, Xinyu Liu, Jin Ma, Zicheng Chi, Jiaqi Ma, and Hongkai Yu. Learning for vehicle-to-vehicle cooperative perception under lossy communication. *IEEE Transactions on Intelligent Vehicles*, 8(4):2650–2660, 2023. 2
- [17] Yiming Li, Bir Bhanu, and Wei Lin. Auction protocol for camera active control. In *2010 IEEE International Conference on Image Processing*, pages 4325–4328. IEEE, 2010. 2
- [18] Yiming Li, Shunli Ren, Pengxiang Wu, Siheng Chen, Chen Feng, and Wenjun Zhang. Learning distilled collaboration graph for multi-agent perception. *Advances in Neural Information Processing Systems*, 34:29541–29552, 2021. 2, 3, 7, 8, 1
- [19] Zhiqi Li, Wenhai Wang, Hongyang Li, Enze Xie, Chonghao Sima, Tong Lu, Yu Qiao, and Jifeng Dai. Bevformer: Learning bird’s-eye-view representation from multi-camera images via spatiotemporal transformers. In *European conference on computer vision*, pages 1–18. Springer, 2022. 1

- [20] Bingyi Liu, Weizhen Han, Enshu Wang, Shengwu Xiong, Chunming Qiao, and Jianping Wang. An efficient message dissemination scheme for cooperative drivings via cooperative hierarchical attention reinforcement learning. *IEEE Transactions on Mobile Computing*, 2023. 1
- [21] Bingyi Liu, Jingxiang Hao, Enshu Wang, Dongyao Jia, Weizhen Han, Libing Wu, and Shengwu Xiong. Multi-agent reinforcement learning based resource allocation for efficient message dissemination in c-v2x networks. In *2024 IEEE/ACM 32nd International Symposium on Quality of Service (IWQoS)*, pages 1–10. IEEE, 2024. 1
- [22] Wei Liu, Lu Xiong, Xin Xia, Yishi Lu, Letian Gao, and Shunhui Song. Vision-aided intelligent vehicle sideslip angle estimation based on a dynamic model. *IET Intelligent Transport Systems*, 14(10):1183–1189, 2020. 1
- [23] Yen-Cheng Liu, Junjiao Tian, Nathaniel Glaser, and Zsolt Kira. When2com: Multi-agent perception via communication graph grouping. In *Proceedings of the IEEE/CVF Conference on computer vision and pattern recognition*, pages 4106–4115, 2020. 2, 3, 7, 8, 1
- [24] Zhijian Liu, Haotian Tang, Alexander Amini, Xinyu Yang, Huizi Mao, Daniela L Rus, and Song Han. Bev-fusion: Multi-task multi-sensor fusion with unified bird’s-eye view representation. In *2023 IEEE international conference on robotics and automation (ICRA)*, pages 2774–2781. IEEE, 2023. 1
- [25] Yifan Lu, Quanhao Li, Baoan Liu, Mehrdad Dianati, Chen Feng, Siheng Chen, and Yanfeng Wang. Robust collaborative 3d object detection in presence of pose errors. In *2023 IEEE International Conference on Robotics and Automation (ICRA)*, pages 4812–4818. IEEE, 2023. 1
- [26] Zhenyang Ni, Zixing Lei, Yifan Lu, Dingju Wang, Chen Feng, Yanfeng Wang, and Siheng Chen. Self-localized collaborative perception. *arXiv preprint arXiv:2406.12712*, 2024. 1
- [27] Adam Paszke, Sam Gross, Francisco Massa, Adam Lerer, James Bradbury, Gregory Chanan, Trevor Killeen, Zeming Lin, Natalia Gimelshein, Luca Antiga, et al. Pytorch: An imperative style, high-performance deep learning library. *Advances in neural information processing systems*, 32, 2019. 6
- [28] Andrea Piazzoni, Jim Cherian, Roshan Vijay, Lap-Pui Chau, and Justin Dauwels. Copem: Cooperative perception error models for autonomous driving. In *2022 IEEE 25th International Conference on Intelligent Transportation Systems (ITSC)*, pages 3934–3939. IEEE, 2022. 2
- [29] Faisal Qureshi and Demetri Terzopoulos. Smart camera networks in virtual reality. *Proceedings of the IEEE*, 96(10):1640–1656, 2008. 2
- [30] Shuyao Shi, Jiahe Cui, Zhehao Jiang, Zhenyu Yan, Guoliang Xing, Jianwei Niu, and Zhenchao Ouyang. Vips: Real-time perception fusion for infrastructure-assisted autonomous driving. In *Proceedings of the 28th annual international conference on mobile computing and networking*, pages 133–146, 2022. 1, 3
- [31] Amanpreet Singh, Tushar Jain, and Sainbayar Sukhbaatar. Learning when to communicate at scale in multiagent cooperative and competitive tasks. *arXiv preprint arXiv:1812.09755*, 2018. 2
- [32] Zhiying Song, Fuxi Wen, Hailiang Zhang, and Jun Li. A cooperative perception system robust to localization errors. In *2023 IEEE Intelligent Vehicles Symposium (IV)*, pages 1–6. IEEE, 2023. 1, 3
- [33] Hao Su, Shin’Ichi Arakawa, and Masayuki Murata. 3d multi-object tracking based on two-stage data association for collaborative perception scenarios. In *2023 IEEE Intelligent Vehicles Symposium (IV)*, pages 1–7. IEEE, 2023. 2
- [34] Sanbao Su, Songyang Han, Yiming Li, Zhili Zhang, Chen Feng, Caiwen Ding, and Fei Miao. Collaborative multi-object tracking with conformal uncertainty propagation. *IEEE Robotics and Automation Letters*, 2024. 2
- [35] Sainbayar Sukhbaatar, Rob Fergus, et al. Learning multiagent communication with backpropagation. *Advances in neural information processing systems*, 29, 2016. 3
- [36] Ming Tan. Multi-agent reinforcement learning: Independent vs. cooperative agents. In *Proceedings of the tenth international conference on machine learning*, pages 330–337, 1993. 2
- [37] A Vaswani. Attention is all you need. *Advances in Neural Information Processing Systems*, 2017. 6
- [38] Tsun-Hsuan Wang, Sivabalan Manivasagam, Ming Liang, Bin Yang, Wenyuan Zeng, and Raquel Urtasun. V2vnet: Vehicle-to-vehicle communication for joint perception and prediction. In *Computer Vision—ECCV 2020: 16th European Conference, Glasgow, UK, August 23–28, 2020, Proceedings, Part II 16*, pages 605–621. Springer, 2020. 1
- [39] Sizhe Wei, Yuxi Wei, Yue Hu, Yifan Lu, Yiqi Zhong, Siheng Chen, and Ya Zhang. Asynchrony-robust collaborative perception via bird’s eye view flow. *Advances in Neural Information Processing Systems*, 36, 2024. 1
- [40] Qi Xie, Xiaobo Zhou, Tie Qiu, Qingyu Zhang, and Wenyu Qu. Soft actor-critic-based multilevel cooperative perception for connected autonomous vehicles.

- IEEE Internet of Things Journal*, 9(21):21370–21381, 2022. 3
- [41] Runsheng Xu, Yi Guo, Xu Han, Xin Xia, Hao Xiang, and Jiaqi Ma. Openoda: an open cooperative driving automation framework integrated with co-simulation. In *2021 IEEE International Intelligent Transportation Systems Conference (ITSC)*, pages 1155–1162. IEEE, 2021. 6
- [42] Runsheng Xu, Hao Xiang, Zhengzhong Tu, Xin Xia, Ming-Hsuan Yang, and Jiaqi Ma. V2x-vit: Vehicle-to-everything cooperative perception with vision transformer. In *European conference on computer vision*, pages 107–124. Springer, 2022. 2, 3, 6, 7, 8, 1
- [43] Runsheng Xu, Hao Xiang, Xin Xia, Xu Han, Jinlong Li, and Jiaqi Ma. Opv2v: An open benchmark dataset and fusion pipeline for perception with vehicle-to-vehicle communication. In *2022 International Conference on Robotics and Automation (ICRA)*, pages 2583–2589. IEEE, 2022. 2, 6, 1
- [44] Runsheng Xu, Weizhe Chen, Hao Xiang, Xin Xia, Lantao Liu, and Jiaqi Ma. Model-agnostic multi-agent perception framework. In *2023 IEEE International Conference on Robotics and Automation (ICRA)*, pages 1471–1478. IEEE, 2023. 3
- [45] Chenyu Yang, Yuntao Chen, Hao Tian, Chenxin Tao, Xizhou Zhu, Zhaoxiang Zhang, Gao Huang, Hongyang Li, Yu Qiao, Lewei Lu, et al. Bevformer v2: Adapting modern image backbones to bird’s-eye-view recognition via perspective supervision. In *Proceedings of the IEEE/CVF Conference on Computer Vision and Pattern Recognition*, pages 17830–17839, 2023. 1
- [46] Dingkan Yang, Kun Yang, Yuzheng Wang, Jing Liu, Zhi Xu, Rongbin Yin, Peng Zhai, and Lihua Zhang. How2comm: Communication-efficient and collaboration-pragmatic multi-agent perception. *Advances in Neural Information Processing Systems*, 36, 2024. 1
- [47] Kun Yang, Dingkan Yang, Jingyu Zhang, Mingcheng Li, Yang Liu, Jing Liu, Hanqi Wang, Peng Sun, and Liang Song. Spatio-temporal domain awareness for multi-agent collaborative perception. In *Proceedings of the IEEE/CVF International Conference on Computer Vision*, pages 23383–23392, 2023.
- [48] Kun Yang, Dingkan Yang, Jingyu Zhang, Hanqi Wang, Peng Sun, and Liang Song. What2comm: Towards communication-efficient collaborative perception via feature decoupling. In *Proceedings of the 31st ACM International Conference on Multimedia*, pages 7686–7695, 2023. 1
- [49] Haibao Yu, Yizhen Luo, Mao Shu, Yiyi Huo, Zebang Yang, Yifeng Shi, Zhenglong Guo, Hanyu Li, Xing Hu, Jirui Yuan, et al. Dair-v2x: A large-scale dataset for vehicle-infrastructure cooperative 3d object detection. In *Proceedings of the IEEE/CVF Conference on Computer Vision and Pattern Recognition*, pages 21361–21370, 2022. 2, 6, 1
- [50] Jingyu Zhang, Kun Yang, Yilei Wang, Hanqi Wang, Peng Sun, and Liang Song. Ermvp: Communication-efficient and collaboration-robust multi-vehicle perception in challenging environments. In *Proceedings of the IEEE/CVF Conference on Computer Vision and Pattern Recognition*, pages 12575–12584, 2024. 3, 7, 8, 1
- [51] Qingzhao Zhang, Xumiao Zhang, Ruiyang Zhu, Fan Bai, Mohammad Naserian, and Z Morley Mao. Robust real-time multi-vehicle collaboration on asynchronous sensors. In *Proceedings of the 29th Annual International Conference on Mobile Computing and Networking*, pages 1–15, 2023. 3
- [52] Qingzhao Zhang, Shuwei Jin, Ruiyang Zhu, Jiachen Sun, Xumiao Zhang, Qi Alfred Chen, and Z Morley Mao. On data fabrication in collaborative vehicular perception: Attacks and countermeasures. In *33rd USENIX Security Symposium (USENIX Security 24)*, pages 6309–6326, 2024. 3
- [53] Xumiao Zhang, Anlan Zhang, Jiachen Sun, Xiao Zhu, Y Ethan Guo, Feng Qian, and Z Morley Mao. Emp: Edge-assisted multi-vehicle perception. In *Proceedings of the 27th Annual International Conference on Mobile Computing and Networking*, pages 545–558, 2021. 1, 3
- [54] Yangheng Zhao, Zhen Xiang, Sheng Yin, Xianghe Pang, Siheng Chen, and Yanfeng Wang. Malicious agent detection for robust multi-agent collaborative perception. *arXiv preprint arXiv:2310.11901*, 2023. 3

mmCooper: A Multi-agent Multi-stage Communication-efficient and Collaboration-robust Cooperative Perception Framework

Supplementary Material

1. Overview

The supplementary material is organized into the following sections:

- Sec. 2: The System Pipeline of mmCooper
- Sec. 3: Additional Experimental Results on OPV2V and DAIR-V2X Datasets
 - Sec. 3.1: Implementation Details
 - Sec. 3.2: Supplements on Localization Errors
 - Sec. 3.3: Supplements on Transmission Delays
 - Sec. 3.4: Robustness to Heading Errors
- Sec. 4: Additional Qualitative Evaluation Results

2. The System Pipeline of mmCooper

The proposed system pipeline of mmCooper is illustrated in Alg. 1. Note that the following pipeline is executed in parallel across all agents. For simplicity, we describe the pipeline from the perspective of the ego agent. The ego agent is represented by i , while the collaborative agents are denoted by j . First, the agent generates BEV features F_{bev}^i and F_{bev}^j through the Observation Module. In the Broadcasting Module, agents generate initial coarse bounding boxes B_{coarse}^i and B_{coarse}^j , where b^i and b^j represent the number of bounding boxes predicted by the ego agent and the collaborating agents, respectively. The collaborative agents then package and broadcast the filtered BEV features along with the coarse bounding boxes. Specifically, $f_{gaussian}(\cdot)$ denotes a Gaussian filter, and $\{F_{bev,m}^j, B_m^j\}$ represents the filtered features and bounding boxes from the collaborative agents.

Subsequently, in the Intermediate-stage Fusion, the ego agent performs feature fusion using the Multi-scale Offset-aware Attention module. The outputs from the fused features at different scales, after undergoing upsampling, are concatenated to obtain the final fused features. Here, $f_{up2}(\cdot)$ and $f_{up3}(\cdot)$ denote the upsampling operations, while $\{F_i^{sc1}, F_i^{sc2}, F_i^{sc3}\}$ represent the feature fusion outputs at three different scales.

In the later-stage fusion, the BBox Filtering & Calibration Module is employed to learn the bounding box offsets and scores. Specifically, DBA refers to the Deformable Bounding Boxes Attention Module, while FFN denotes the feed-forward network, $f_{enc,b}(\cdot)$ represents the feature extractor for bounding boxes, $f_{off}(\cdot)$ is the offset mapping function, and $f_{score}(\cdot)$ is the score mapping function. $\varphi(\cdot)$ represents the filtering and calibration through scores and offsets.

Finally, the fused features are input into a detection head to predict the fused bounding box \mathcal{B}_{fused} . The final bounding box is composed of the initial prediction, the bounding box predicted from the fused features, and the bounding box obtained after filtering and calibration from collaborative agents. $f_{post}(\cdot)$ represents the combination of all bounding boxes.

3. Additional Experimental Results on OPV2V and DAIR-V2X Datasets

In this section, we provide additional experiments to supplement the results on the datasets OPV2V[43] and DAIR-V2X[49] presented in the *main paper*.

3.1. Implementation Details

On the OPV2V and DAIR-V2X datasets, the dimensions of the voxels encoded by the encoder are $0.4 \times 0.4 \times 4$. The shape of the shared BEV features among agents is (64, 100, 252) for DAIR-V2X and (64, 100, 352) for OPV2V. The shared bounding boxes among agents are represented by their center coordinates, dimensions (length, width, height), and heading angle. The detection decoder consists of two distinct 1×1 convolutional layers.

3.2. Supplements on Localization Errors

The localization errors on the OPV2V and DAIR-V2X datasets are sampled from a Gaussian distribution with a mean of 0 m and a standard deviation $\sigma \in \{0.0, 0.1, 0.2, 0.3, 0.4\}m$. The experimental results, as shown in Figure 7, demonstrate that our proposed mmCooper outperforms the existing state-of-the-art methods[11, 18, 23, 42, 50] across different levels of localization error, highlighting its robustness to such errors.

3.3. Supplements on Transmission Delays

We evaluated the performance of the models on the OPV2V and DAIR-V2X datasets under transmission delays for $\{0, 100, 200, 300, 400\}ms$. As shown in Figure 8, our proposed mmCooper consistently outperforms the existing state-of-the-art methods across all transmission delay conditions, demonstrating the superiority of our approach in scenarios with transmission delays.

dui

3.4. Robustness to Heading Errors.

Figure 9 demonstrates the performance of our proposed mmCooper method compared to other baseline methods un-

Algorithm 1 System Pipeline of the Proposed mmCooper

Define $N = \{1, \dots, n\}$ as the agent set, $i \in N$ represents the ego agent, while $j \in N$ denotes the collaborative agents. $X_{i/j}$ serves as the input point cloud.

For collaborative agents.**# Observation Module.****for each agent $j \in N$, do**

$$X'_j = T_{j \rightarrow i} \cdot X_j$$

$$F_{bev}^j = \psi_{encoder}(X'_j) \in \mathbb{R}^{C \times H \times W}$$

end for**# Broadcasting Module.****for each $j \in N$, do**

$$B_{coarse}^j = f_{dec}(F_{bev}^j) \in \mathbb{R}^{b^j \times 7}$$

$$C_f^j, C_b^j = \phi_{conf}(F_{bev}^j)$$

$$C_f^j, C_b^j = f_{gaussian}(C_f^j, C_b^j)$$

$$M_{f,top}^j, M_{b,top}^j = f_{top}(C_f^j, C_b^j)$$

$$M_{f,g}^j, M_{b,g}^j = f_{max}\left(\frac{\exp((\log C_{f/b}^j + g_f)/\tau)}{\sum_s \exp((\log C_s^j + g_s)/\tau)}\right)$$

$$\mathcal{M}_{f/b}^j = M_{f/b,g}^j \odot M_{f/b,top}^j$$

$$F_{bev,m}^j = \mathcal{M}_f^j \odot F_{bev}^j; B_m^j = \mathcal{M}_b^j \odot B_{coarse}^j$$

broadcast $\{F_{bev,m}^j, B_m^j\}$ to other agent**end for****# For ego agent.****# Observation Module.**

$$F_{bev}^i = \psi_{encoder}(X_i) \in \mathbb{R}^{C \times H \times W}$$

Broadcasting Module.

$$B_{coarse}^i = f_{dec}(F_{bev}^i) \in \mathbb{R}^{b^i \times 7}$$

Intermediate-stage Fusion.Receive $\{F_{bev,m}^j, B_m^j\}$ sent by collaborative agents.Encode the feature set $\{F_{bev}^i, F_{bev,m}^j\}$ into three scales $S = \{sc1, sc2, sc3\}$.**For each $sc \in S$, do**

$$\mathcal{F}_{i,c}^{sc} = CrossAttn(\sigma(F_{bev,c}^{i,sc}), F_{bev,c}^{j,s \times s, sc}, F_{bev,c}^{j,s \times s, sc})$$

end for

$$\mathcal{F}_i = concat(\mathcal{F}_i^{sc1}, f_{up2}(\mathcal{F}_i^{sc2}), f_{up3}(\mathcal{F}_i^{sc3}))$$

Late-stage Fusion.

$$F_b(q) = f_{enc,b}(B_{i,m})$$

$$DBA(q) = \sum_{\alpha=1}^A W_{\alpha} [\sum_{n=1}^N \sum_{m=1}^M \omega(W_{\beta} F_b(q)) F_j(q + \Delta q_m)]$$

$$F_{DBA} = DBA(q) + \mathcal{F}_i$$

$$F_{DBA} = FFN(F_{DBA}) + F_{DBA}$$

$$off, score = f_{off}(F_{DBA}), f_{score}(F_{DBA})$$

$$\mathcal{B}_m^j = \varphi(off, score, B_m^j)$$

Detection Decoders

$$\mathcal{B}_{fused} = f_{dec}(\mathcal{F}_i)$$

$$\mathcal{B}_{final}^i = f_{post}(B_{coarse}^i, \mathcal{B}_m^j, \mathcal{B}_{fused})$$

der varying levels (i.e., $\{0.0, 0.2, 0.4, 0.6, 0.8\}^\circ$) of heading error noise on the OPV2V and DAIR-V2X datasets. As illustrated in Figure 9, the performance of all models

decreases as the heading errors increase. However, mmCooper consistently outperforms the current state-of-the-art models across all error levels, highlighting the advantages

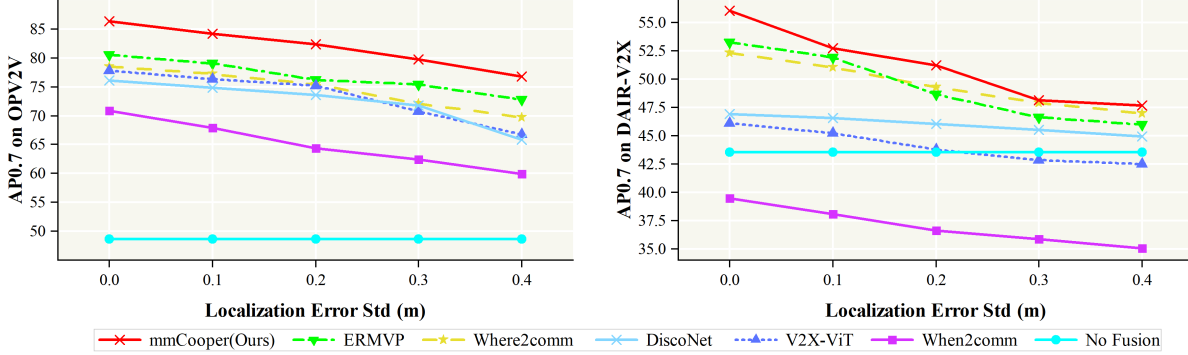


Figure 7. Robustness to the localization error on the OPV2V and DAIR-V2X datasets.

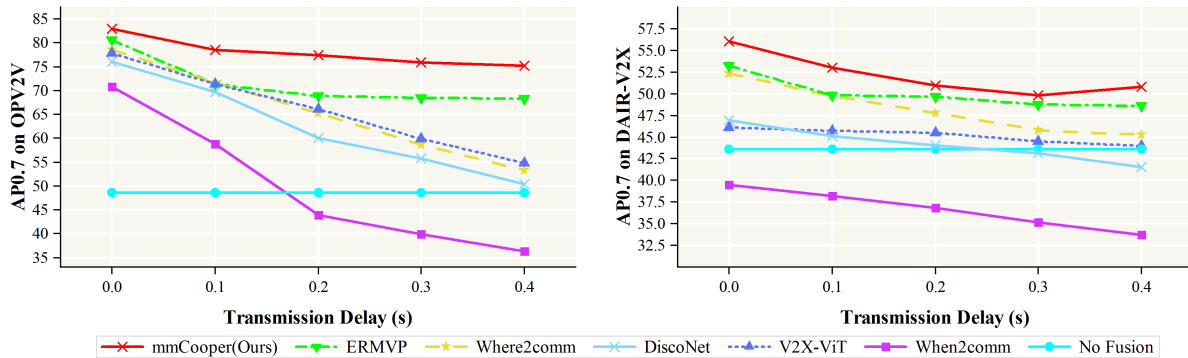


Figure 8. Robustness to the transmission delay on the OPV2V and DAIR-V2X datasets.

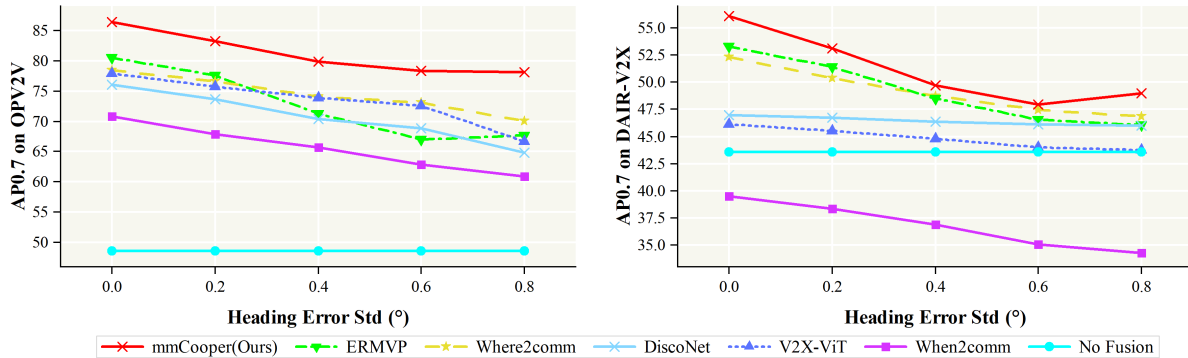


Figure 9. Robustness to the heading error on the OPV2V and DAIR-V2X datasets.

of our designed Multi-Scale Offset-Aware Fusion Module and BBox Filtering & Calibration Module in enhancing system robustness.

4. Additional Qualitative Evaluation Results

We provide additional qualitative results on DAIR-V2X datasets. Figures 10 present visualizations of different road scenarios. Our proposed mmCooper method can detect almost all ground truths without any false positives. The re-

sults demonstrate that our proposed mmCooper achieves outstanding detection performance across various scenarios.

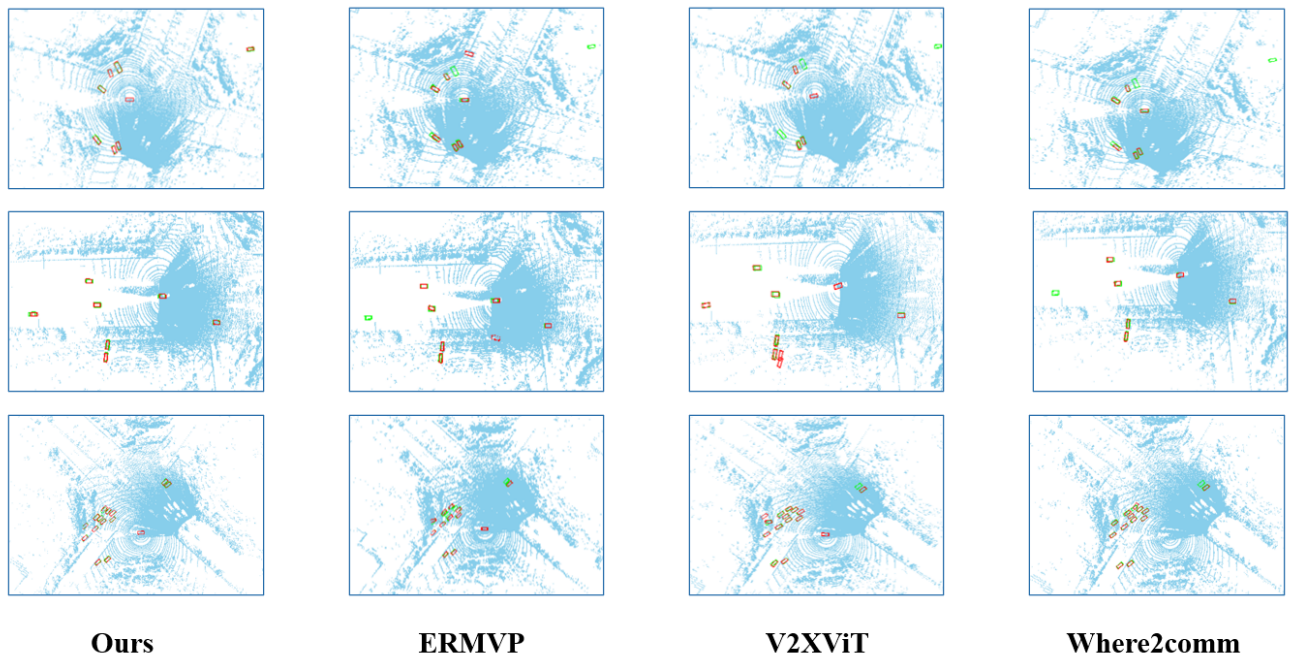


Figure 10. More visualization comparison of detection results on the DAIR-V2X dataset. Green and red boxes represent the ground truth and the model-predicted bounding boxes, respectively.